ELSEVIER

Journal of Biomechanics 41 (2008) 1458–1466

JOURNAL OF BIOMECHANICS

www.elsevier.com/locate/jbiomech
www.JBiomech.com

# A variational constitutive model for soft biological tissues

Tamer El Sayed[a], Alejandro Mota[a], Fernando Fraternali[b], Michael Ortiz[a,*]

[a]*Division of Engineering and Applied Science, California Institute of Technology, Pasadena, CA 91125, USA*
[b]*Department of Civil Engineering, University of Salerno, 84084 Fisciano (SA), Italy*

Accepted 18 February 2008

**Abstract**

In this paper, a fully variational constitutive model of soft biological tissues is formulated in the finite strain regime. The model includes Ogden-type hyperelasticity, finite viscosity, deviatoric and volumetric plasticity, rate and microinertia effects. Variational updates are obtained via time discretization and pre-minimization of a suitable objective function with respect to internal variables. Genetic algorithms are used for model parameter identification due to their suitability for non-convex, high dimensional optimization problems. The material behavior predicted by the model is compared to available tests on swine and human brain tissue. The ability of the model to predict a wide range of experimentally observed behavior, including hysteresis, cyclic softening, rate effects, and plastic deformation is demonstrated.


*Keywords:* Biological tissues; Variational; Ogden; Plasticity; Shear; Volumetric damage; Finite strain; Cavitation; Genetic algorithms; Hyper elasticity; Viscosity; Microinertia

## 1. Introduction

Soft biological tissues exhibit complex mechanical behavior, characterized by large strains, rate-sensitivity, hysteresis, solid/fluid behavior, residual stresses, and permanent deformation. They consist of cells, extracellular components, vascular network, and water. One important example is brain tissue, which exhibits extremely soft behavior and is often modeled using hyperelastic or hyperviscoelastic constitutive equations (Prange and Margulies, 2002; Miller and Chinzei, 1997, 2002; Miller et al., 2006; Meaney, 2003; Brands et al., 2002; Velardi et al., 2006). Hyperelastic or viscoelastic anisotropic models for arterial tissues have been proposed by Holzapfel, Ogden and Gasser in a series of recent studies (Holzapfel et al., 2000; Holzapfel, 2001; Gasser et al., 2006). Some authors have analyzed plasticity, hysteresis, permanent deformation and biphasic (solid/fluid) behavior of soft biological tissues (Bergström and Boyce, 2001; Gasser and Holzapfel, 2002; Franceschini et al., 2006). Variationally consistent finite viscoelastic models for rubber-like materials have been proposed by several authors (Govindjee and Reese, 1997; Reese and Govindjee, 1998; Fancello et al., 2006). It is often assumed that biological tissues exhibit mechanical *anisotropy*, due to the presence of reinforcing fibers in the extracellular matrix (Prange and Margulies, 2002; Meaney, 2003; Ogden, 2003; Gasser et al., 2006; Velardi et al., 2006). Nevertheless, some authors argue that "very soft tissue do not bear mechanical load and do not exhibit directional structure (provided that a large enough sample is considered ...)" (see Miller, 2005 and references therein).

Two of the major recognized causes of physiological damage to living tissues are tensile and shearing structural failures caused by relative motions within the tissues (Stoyanovski and Grozeva, 2005). For example, referring to head traumas, linear forces resulting from straight ahead acceleration–deceleration impact can be associated with focal lesions and tensile (cavitation) injuries. Those may occur at the site of contact (coup injury) or distant, usually opposite the site of contact (contre-coup injury) (Lubock and Goldsmith, 1980; Hardy et al., 1994; Nusholtz et al., 1996; Brennen, 2003; Johnson and Young,

*Corresponding author. Tel.: +1 626 395 4530.
*E-mail addresses:* tamer@caltech.edu (T. El Sayed), ortiz@aero.caltech.edu (M. Ortiz).

0021-9290/$ - see front matter © 2008 Elsevier Ltd. All rights reserved.
doi:10.1016/j.jbiomech.2008.02.023

2006). Rotational forces produced by rotational acceleration–deceleration traumas can instead lead to shearing injuries in the brain parenchyma, between tissue planes of varying densities (diffuse axonal injury) (Strich, 1956; Adams and Graham, 1984; Perles and Rewcastle, 1967).

In view of all the above requirements in the modeling of soft biological tissues, herein we present a fully variational phenomenological constitutive model with the ability to capture all of the following:

- Rate and microinertia effects.
- Complex viscous behavior via a flexible number of viscoelastic mechanisms capable of representing finite viscosity.
- Hysteresis, deviatoric and volumetric plasticity.
- Strong non-linearity, different behavior in tension and compression, preconditioning and cyclic softening.
- Thermal softening and adiabatic heating via thermal updates.
- Void growth and shrinkage during the process of cavitation (El Sayed et al., 2007).

The rheological representation of the model consists of an elastoplastic network acting in parallel with several viscoelastic networks. Quasi-incompressible Ogden-type potentials govern the elastic behavior, both in the elastoplastic (which accounts for both deviatoric and volumetric plasticity) and viscoelastic branches. The Ogden model was chosen because it can reduce to either the Neo-Hookean model ($N=1$, $\alpha=2$), or the Mooney–Rivlin model ($N=2$, $\alpha_1=2$, $\alpha_2=-2$). This indeed shows that the Ogden model is a practical choice in this framework due to its generality and capability to reproduce simpler existing models, if needed, in such an easy fashion. Cyclic stress softening is reproduced through a combination of elastoplastic and viscoelastic responses. Deviatoric plasticity allows for representing shearing-type injuries, while volumetric plasticity is intended to reproduce cavitation injuries, being related to the expansion of spherical voids or bubbles in a plastically incompressible matrix (El Sayed et al., 2007). As the pressure reaches a critical value in tension, the material is allowed to yield and exhibit volumetric strain softening. Ortiz and Molinari (1992) analyzed the dynamic expansion of a single spherical void in an infinite rigid plastic medium under the action of remote hydrostatic tension. They reported that if the initial void radius increases by at least one order of magnitude, the void growth is dominated by microinertial effects, whereas the effect of rate dependence of the material and the plastic dissipative effects play a secondary role. High accelerations sustained by the material particles in the vicinity of voids result in significant inertial effects, particularly for materials with low strain-rate sensitivity (Molinari and Mercier, 2001). The presented model accounts for microinertia (see Section 2.4). This particular feature is utilized in the simulation of traumatic brain injury (El Sayed et al., 2007) where volumetric damage as a result of a high strain rate impact is evident. Viscous deformation of the viscoelastic networks allows one to reproduce transient deviatoric and volumetric damage to the tissue.The model is formulated in an isotropic framework and is intended to mimic the presence of reinforcing fibers through regional dependence of mechanical properties (Prange and Margulies, 2002).

The number of model parameters is a function of the number of active Ogden terms and relaxation mechanisms, and therefore a significant number of parameters may need to be identified. This requires the use of advanced techniques for the calibration of model parameters based on experimental data, hence we propose a procedure based on genetic algorithms (GA), which have been proved to be well suited for multimodal non-convex optimization (Schmitt, 2004). Several sets of experimental data are compared with model predictions, showing the ability of the model to reproduce the observed behavior of soft biological tissues. Monotonic and cyclic tests on brain tissue are examined, which involve complex behavior such as cyclic hysteresis, cyclic softening, rate effects, and plastic deformation.

The current constitutive model is applied to the finite element simulation of diffuse axonal injury and cavitation damage associated with traumatic brain injury in El Sayed et al. (2007).

## 2. Constitutive model

Let $\boldsymbol{F}$ denote the deformation gradient at an arbitrary point of the material, and let

$$\boldsymbol{F}=\boldsymbol{F}^e\boldsymbol{F}^p=\boldsymbol{F}^e_1\boldsymbol{F}^v_1=\cdots=\boldsymbol{F}^e_M\boldsymbol{F}^v_M \tag{2.1}$$

be its multiple multiplicative decomposition, where $M$ is a positive integer that defines the number of viscoelastic (Maxwell-type) relaxation networks that the model possesses, and that act in parallel with an elastoplastic equilibrium network; $\boldsymbol{F}^e,\boldsymbol{F}^e_1,\ldots,\boldsymbol{F}^e_M$ are the elastic parts of $\boldsymbol{F}$; $\boldsymbol{F}^p$ is the plastic deformation gradient; and $\boldsymbol{F}^v_1,\ldots,\boldsymbol{F}^v_M$ are the viscous deformation gradients.

The thermo-mechanical behavior of the material derives from the additive potential

$$A=A^{ep}(\boldsymbol{F},\boldsymbol{F}^p,\boldsymbol{Z}^p,T)+A^{ve}(\boldsymbol{F},\boldsymbol{F}^v_i,\boldsymbol{Z}^v_i), \tag{2.2}$$

where $A^{ep}$ and $A^{ve}$ are elastoplastic and viscoelastic contributions, correspondingly; $\boldsymbol{Z}^p$ is a vector of plastic internal variables; $\boldsymbol{Z}^v_i$ are vectors of viscous internal variables ($i=1,\ldots,M$); and $T$ is the absolute temperature.

The first Piola–Kirchhoff stress $\boldsymbol{P}$, and the thermodynamic forces $\boldsymbol{Y}^p$ and $\boldsymbol{Y}^v_i$ conjugate to $\boldsymbol{Z}^p$ and $\boldsymbol{Z}^v_i$ follow from

$$\boldsymbol{P}=\frac{\partial A}{\partial \boldsymbol{F}}, \tag{2.3}$$

$$\boldsymbol{Y}^p=-\frac{\mathrm{d}A}{\mathrm{d}\boldsymbol{Z}^p}, \tag{2.4}$$

$$\boldsymbol{Y}^v_i=-\frac{\mathrm{d}A}{\mathrm{d}\boldsymbol{Z}^v_i}. \tag{2.5}$$

The free energy is assumed to have the additive structure

$$A^{ep}(\boldsymbol{F},\boldsymbol{F}^p,\boldsymbol{Z}^p,T)+A^{ve}(\boldsymbol{F},\boldsymbol{F}_i^v,\boldsymbol{Z}_i^v) = W^e(\boldsymbol{F}\boldsymbol{F}^{p-1},T)+W^p(\boldsymbol{Z}^p,T) + \sum_{i=1}^{M} W_i^e(\boldsymbol{F}\boldsymbol{F}_i^{v-1},T)+\rho_0 C_v T\left(1-\log\frac{T}{T_0}\right), \tag{2.6}$$

where $W^e$ is the elastic strain-energy density associated with the elastoplastic branch; $W^p$ is the plastic stored energy; $W_i^e$ $(i=1,\ldots,M)$ are the elastic strain-energy densities corresponding to the viscous relaxation mechanisms; $\rho_0$ is the mass density per unit undeformed volume; $C_v$ is the specific heat per unit mass at constant volume and $T_0$ is the reference temperature.

The internal variables $\boldsymbol{F}^p$, $\boldsymbol{Z}^p$ and $\boldsymbol{F}_i^v$, $\boldsymbol{Z}_i^v$ are closely related to each other by the means of suitable differential equations or *flow rules* to be introduced later.

### 2.1. Ogden-type hyperelasticity

It is assumed that the elastic strain energies admit a decomposition into deviatoric and volumetric parts. Furthermore, it proves convenient for the constitutive updates to introduce the logarithmic elastic strain measures

$$\boldsymbol{\varepsilon}^e=\tfrac{1}{2}\log(\boldsymbol{F}^{e\mathrm{T}}\boldsymbol{F}^e)=\tfrac{1}{2}\log(\boldsymbol{F}^{p-\mathrm{T}}\boldsymbol{C}\boldsymbol{F}^{p-1}), \tag{2.7}$$

$$\boldsymbol{\varepsilon}_i^e=\tfrac{1}{2}\log(\boldsymbol{F}_i^{e\mathrm{T}}\boldsymbol{F}_i^e)=\tfrac{1}{2}\log(\boldsymbol{F}_i^{v-\mathrm{T}}\boldsymbol{C}\boldsymbol{F}_i^{v-1}), \tag{2.8}$$

$$\boldsymbol{e}^e=\mathrm{dev}(\boldsymbol{\varepsilon}^e),\quad \theta^e=\mathrm{tr}(\boldsymbol{\varepsilon}^e), \tag{2.9}$$

$$\boldsymbol{e}_i^e=\mathrm{dev}(\boldsymbol{\varepsilon}_i^e),\quad \theta_i^e=\mathrm{tr}(\boldsymbol{\varepsilon}_i^e), \tag{2.10}$$

where $\boldsymbol{C}$ is the right Cauchy–Green deformation tensor ($\boldsymbol{C}=\boldsymbol{F}^{\mathrm{T}}\boldsymbol{F}$), and dev$(\cdot)$ and tr$(\cdot)$ are the deviator and the trace operators, respectively. Thus, the elastic strain-energy density decompositions are

$$W^e(\boldsymbol{\varepsilon}^e,T)=W^{e,\mathrm{vol}}(\theta^e,T)+W^{e,\mathrm{dev}}(\boldsymbol{e}^e,T), \tag{2.11}$$

$$W_i^e(\boldsymbol{\varepsilon}_i^e,T)=W_i^{e,\mathrm{vol}}(\theta_i^e,T)+W_i^{e,\mathrm{dev}}(\boldsymbol{e}_i^e,T), \tag{2.12}$$

with

$$W^{e,\mathrm{vol}}(\theta^e,T)=\frac{\kappa}{2}[\theta^e-\alpha(T-T_0)]^2, \tag{2.13}$$

$$W^{e,\mathrm{dev}}(\boldsymbol{e}^e,T)=\sum_{j=1}^{3}\sum_{n=1}^{N}\frac{\mu_n}{\alpha_n}([\exp(e_j^e)]^{\alpha_n}-1), \tag{2.14}$$

$$W_i^{e,\mathrm{vol}}(\theta_i^e,T)=\frac{\kappa_i}{2}(\theta_i^e)^2, \tag{2.15}$$

$$W_i^{e,\mathrm{dev}}(\boldsymbol{e}_i^e,T)=\sum_{j=1}^{3}\sum_{n=1}^{N_i}\frac{\mu_{i,n}}{\alpha_{i,n}}([\exp(e_{i,j}^e)]^{\alpha_{i,n}}-1). \tag{2.16}$$

In (2.11)–(2.16), $\kappa$ and $\kappa_i$ $(i=1,\ldots,M)$ are bulk moduli; $\mu_n$ and $\mu_{i,n}$ are shear moduli associated with the Ogden potentials (Ogden, 1984) adopted for deviatoric elasticity; $\alpha_n$ and $\alpha_{i,n}$ are dimensionless real parameters; $N$ is the number of Ogden terms considered for the time-infinity behavior; $N_i$ is the number of Ogden terms selected for the $i$th relaxation mechanism; $e_j^e$ and $e_{i,j}^e$ $(j=1,2,3)$ are the eigenvalues of $\boldsymbol{e}^e$ and $\boldsymbol{e}_i^e$, respectively.

Polyconvexity of the Ogden models requires the following according to (Ball, 1977; Ciarlet, 1998):

$$\mu_n\alpha_n>0,\quad |\alpha_n|>1,\quad \forall n=1,\ldots,N, \tag{2.17}$$

$$\mu_{i,n}\alpha_{i,n}>0,\quad |\alpha_{i,n}|>1,\quad \forall n=1,\ldots,N_i,\ \forall i=1,\ldots,M. \tag{2.18}$$

For convenience, let

$$\mu^0=\frac{1}{2}\left(\sum_{n=1}^{N}\mu_n\alpha_n+\sum_{i=1}^{M}\sum_{n=1}^{N_i}\mu_{i,n}\alpha_{i,n}\right), \tag{2.19}$$

$$\mu^\infty=\frac{1}{2}\sum_{n=1}^{N}\mu_n\alpha_n \tag{2.20}$$

denote the consistent shear moduli in the small strain regime, which correspond to initial and long term behaviors, respectively.

### 2.2. Deviatoric and volumetric plasticity

The plastic stored energy is also assumed to admit an additive decomposition into volumetric and deviatoric parts as

$$W^p(\boldsymbol{Z}^p,T)=W^{p,\mathrm{vol}}(\theta^p,T)+W^{p,\mathrm{dev}}(\varepsilon^p,T), \tag{2.21}$$

where

$$\boldsymbol{Z}^p=\{\theta^p,\varepsilon^p\}, \tag{2.22}$$

in which $\theta^p\geqslant 0$ and $\varepsilon^p\geqslant 0$ are effective volumetric and deviatoric plastic strains, respectively. The flow rule that relates $\boldsymbol{Z}^p$ and $\boldsymbol{F}^p$ is assumed to be

$$\dot{\boldsymbol{F}}^p\boldsymbol{F}^{p-1}=\dot{\theta}^p\boldsymbol{N}^p+\dot{\varepsilon}^p\boldsymbol{M}^p, \tag{2.23}$$

where $\boldsymbol{M}^p$ and $\boldsymbol{N}^p$ are second order tensors subject to the normality constraints

$$\mathrm{tr}(\boldsymbol{M}^p)=0,\quad \boldsymbol{M}^p\cdot\boldsymbol{M}^p=\tfrac{3}{2},\quad \boldsymbol{N}^p=\pm\tfrac{1}{3}\boldsymbol{I}. \tag{2.24}$$

Irreversibility of plastic flow requires

$$\dot{\varepsilon}^p\geqslant 0,\quad \dot{\theta}^p\geqslant 0. \tag{2.25}$$

#### 2.2.1. Deviatoric plasticity

The deviatoric plastic behavior is modeled via the hardening power law

$$W^{p,\mathrm{dev}}(\varepsilon^p,T)=\frac{n\,\sigma_0(T)\varepsilon_0^p}{n+1}\left(1+\frac{\varepsilon^p}{\varepsilon_0^p}\right)^{(n+1)/n}, \tag{2.26}$$

where $n$ is the hardening exponent, $\sigma_0(T)$ is the yield stress, and $\varepsilon_0^p$ is the reference deviatoric plastic strain. Furthermore, the yield stress is assumed to be a function

of temperature

$$\sigma_0(T) = \sigma_0(T_0)\left(1 - \frac{T - T_0}{T_m - T_0}\right)^l, \tag{2.27}$$

where $T_0$ is the reference temperature, $T_m$ is the melting temperature and $l$ is the thermal softening exponent.

### 2.2.2. Volumetric plasticity

We assume that the volumetric plastic behavior is related to the expansion or collapse of spherical voids in a plastically incompressible matrix (Ortiz and Molinari, 1992; Weinberg et al., 2006; Weinberg and Ortiz, 2005). The initial void volume fraction of the body in the undeformed configuration is given by

$$f_0 = N_v \frac{4\pi a_0^3}{3}, \tag{2.28}$$

where $N_v$ is the void density (number of voids per unit undeformed volume); and $a_0$ is the initial void radius.

Neglecting the elastic volume change of the voids, the plastic volumetric deformation can be expressed as a function of the void radius

$$J^p = 1 - f_0 + N_v \frac{4\pi a^3}{3}, \quad f = \frac{f_0 + J^p - 1}{J^p}, \tag{2.29}$$

where $J^p$ is the determinant of $\boldsymbol{F}^p$, and $a$ is the void radius in the deformed configuration. For purely volumetric deformations the flow rule (2.23) becomes

$$\frac{\mathrm{d}}{\mathrm{d}t}\log J^p = \mathrm{tr}(\boldsymbol{N}^p)\dot{\theta}^p = \pm\dot{\theta}^p, \tag{2.30}$$

which implies

$$\dot{\theta}^p = \left|\frac{\mathrm{d}}{\mathrm{d}t}\log J^p\right|, \tag{2.31}$$

which in turn means that the internal variable $\theta^p$ represents a measure of the accumulated volumetric plastic deformation. By introducing the expression of the stored energy of a single spherical void in a power-law hardening material (Ortiz and Molinari, 1992), and integrating the energies stored by each void (*dilute limit*), we obtain

$$W^{p,\mathrm{vol}}(\theta^p, T) = \frac{n\sigma_0(T)\varepsilon_0^p}{n+1} N_v \frac{4\pi a^3}{3} g(\theta^p, n), \tag{2.32}$$

where

$$g(\theta^p, n) = \int_1^{1/f} \left(1 + \frac{2}{3\varepsilon_0^p} \times \log\frac{x}{x - 1 + f_0/(f_0 + \exp\theta^p - 1)}\right)^{(n+1)/n} \mathrm{d}x \tag{2.33}$$

## 2.3. Evolution laws—rate effects

Evolution laws for the internal variables are obtained variationally by assuming the existence of differentiable kinetic potentials $\psi(\boldsymbol{Y}^p, \boldsymbol{F}^p, T)$ and $\phi_i(\boldsymbol{Y}_i^v, \boldsymbol{F}_i^v, T)$ such that

$$\dot{\boldsymbol{Z}}^p = \frac{\partial\psi}{\partial\boldsymbol{Y}^p}, \quad \dot{\boldsymbol{Z}}_i^v = \frac{\partial\phi_i}{\partial\boldsymbol{Y}_i^v} \quad (i = 1, \ldots, M), \tag{2.34}$$

where $\boldsymbol{Z}^p = \{\theta^p, \varepsilon^p\}$, $\boldsymbol{Z}_i^v = \{\varepsilon_{i,1}^v, \varepsilon_{i,2}^v, \varepsilon_{i,3}^v\}$, $\dot{\varepsilon}_{i,j}^v$ being the eigenvalues of $\boldsymbol{d}_i^v = \dot{\boldsymbol{F}}_i^v \boldsymbol{F}_i^{v-1}$, while $\boldsymbol{Y}^p = \{Y^p, Z^p\}$ and $\boldsymbol{Y}_i^v = \{\sigma_{i,1}^v, \sigma_{i,2}^v, \sigma_{i,3}^v\}$ are the thermodynamic forces defined in the appendix.

The dual kinetic potentials $\psi^*(\boldsymbol{F}^p, \dot{\boldsymbol{Z}}^p, T)$, $\phi_i^*(\boldsymbol{F}_i^v, \dot{\boldsymbol{Z}}_i^v, T)$ are introduced via the Legendre transformations

$$\psi^*(\boldsymbol{F}^p, \dot{\boldsymbol{Z}}^p, T) = \sup_{\boldsymbol{Y}^p}\{\boldsymbol{Y}^p \cdot \dot{\boldsymbol{Z}}^p - \psi(\boldsymbol{Y}^p, \boldsymbol{F}^p, T)\}, \tag{2.35}$$

$$\phi_i^*(\boldsymbol{F}_i^v, \dot{\boldsymbol{Z}}_i^v, T) = \sup_{\boldsymbol{Y}_i^v}\{\boldsymbol{Y}_i^v \cdot \dot{\boldsymbol{Z}}_i^v - \phi(\boldsymbol{Y}_i^v, \boldsymbol{F}_i^v, T)\} \quad (i = 1, \ldots, M), \tag{2.36}$$

that in turn satisfy

$$\boldsymbol{Y}^p = \frac{\partial\psi^*}{\partial\dot{\boldsymbol{Z}}^p}, \quad \boldsymbol{Y}_i^v = \frac{\partial\phi_i^*}{\partial\dot{\boldsymbol{Z}}_i^v}. \tag{2.37}$$

The dual kinetic potentials may also be decomposed into deviatoric and volumetric components

$$\psi^*(\boldsymbol{F}^p, \dot{\boldsymbol{Z}}^p, T) = \psi^{*,\mathrm{vol}}(J^p, \dot{\theta}^p, T) + \psi^{*,\mathrm{dev}}(\dot{\varepsilon}^p, T), \tag{2.38}$$

$$\phi_i^*(\boldsymbol{F}_i^v, \dot{\boldsymbol{Z}}_i^v, T) = \phi_i^{*,\mathrm{vol}}(\dot{\theta}_i^v, T) + \phi_i^{*,\mathrm{dev}}(\dot{e}_i^v, T), \tag{2.39}$$

where

$$\psi^{*,\mathrm{vol}}(J^p, \dot{\theta}^p, T) = \frac{m^2\sigma_0(T)\dot{\varepsilon}_0^p}{m+1} N_v \frac{4\pi a^3}{3}(1 - f^{1/m})\left|\frac{2\dot{a}}{\dot{\varepsilon}_0^p a}\right|^{(m+1)/m}, \tag{2.40}$$

$$\psi^{*,\mathrm{dev}}(\dot{\varepsilon}^p, T) = \frac{m^2\sigma_0(T)\dot{\varepsilon}_0^p}{m+1}\left(\frac{\dot{\varepsilon}^p}{\dot{\varepsilon}_0^p}\right)^{(m+1)/m}, \tag{2.41}$$

$$\phi_i^{*,\mathrm{vol}}(\dot{\theta}_i^v, T) = \frac{\eta_i^{\mathrm{vol}}}{2}\dot{\theta}_i^{v\,2}, \tag{2.42}$$

$$\phi_i^{*,\mathrm{dev}}(\dot{e}_i^v, T) = \sum_{j=1}^{3}\sum_{n=1}^{N_i}\frac{\eta_{i,n}^{\mathrm{dev}}}{\alpha_{i,n}}([\exp(\dot{e}_{i,j}^v)]^{\alpha_{i,n}} - 1). \tag{2.43}$$

In (2.40) and (2.41) $m$ is the rate-sensitivity exponent; $\dot{\varepsilon}_0^p$ is the reference plastic strain rate; and the void radius $a$ is regarded as a function of $J^p$ through (2.29). The rates $\dot{J}^p$ and $\dot{\theta}^p$ are related through (2.31). In (2.42) and (2.43) $\eta_i^{\mathrm{vol}}$ and $\eta_{i,n}^{\mathrm{dev}}$ are the volumetric and deviatoric viscous coefficients, respectively ($i = 1, \ldots, M; n = 1, \ldots, N_i$). Non-Newtonian viscosity may be modeled by assuming that these coefficients are deformation dependent.

## 2.4. Microinertia

The microinertia attendant to the plastic expansion of voids is regarded as dissipated energy in a system of shell-like particles with variable mass (Ortiz and Molinari, 1992; Weinberg et al., 2006). Reformulation of this problem into

an equivalent system of particles with constant mass leads to a microkinetic energy of the form (Weinberg et al., 2006):

$$L(b,\dot{b}) = \frac{3}{2}\rho_{v_0}\dot{b}^2, \quad \rho_{v_0} = \rho_0 N_v \frac{4\pi a_0^3}{3}, \quad b = \frac{2}{5}\frac{a^{5/2}}{a_0^{3/2}}. \tag{2.44}$$

The introduction of microinertia effects a change in the thermodynamic stress $\boldsymbol{T}^p$

$$\boldsymbol{T}^p = \boldsymbol{F}^{eT}\boldsymbol{P} - A_{,\boldsymbol{F}^p} + \left(\frac{\partial L}{\partial \boldsymbol{F}^p} - \frac{\mathrm{d}}{\mathrm{d}t}\frac{\partial L}{\partial \dot{\boldsymbol{F}}^p}\right). \tag{2.45}$$

The reader should refer to the appendix for details on the incremental updates.

## 3. Parameters identification via GA

We present in this section a parameter identification method via GA. The identification procedure assumes that a collection of $N^e$ experimental results is available for model parameter identification, through a data set of the form

$$\{[x_i^e, \bar{y}_i^e]_{i=1,\ldots,N_p^e}\}^{e=1,\ldots,N^e}, \tag{3.1}$$

where $x_i^e$ are experimental observations of a suitable *strain measure* $x$, and $\bar{y}_i^e$ are the corresponding recordings of a *stress measure* $y$, and $N_p^e$ is the number of data points for experiment $e$. The best-fit values of selected parameters

$$\boldsymbol{p} = \{\{p_m\}_{m=1,\ldots,P}\} \tag{3.2}$$

are sought, under simple bounds of the form

$$\boldsymbol{p} \in D = [p_1^{lb}, p_1^{ub}] \times \cdots \times [p_P^{lb}, p_P^{ub}]. \tag{3.3}$$

If $\boldsymbol{p}$ is assigned, numerical simulations of the experiments can be employed to get a set of predictions

$$\{\{x_i^e, y_i^e(\boldsymbol{p})\}_{i=1,\ldots,N_p^e}\}^{e=1,\ldots,N^e}, \tag{3.4}$$

and their fitting performance can be evaluated through the *fitness function*

$$f(\boldsymbol{p}) = \max_i |y_i^e(\boldsymbol{p}) - \bar{y}_i^e|, \tag{3.5}$$

which is an $L_\infty$ norm of the residuals $y^e - \bar{y}^e$. This leads to the multivariate minimization problem

$$\min_{\boldsymbol{p}\in D} f(\boldsymbol{p}), \tag{3.6}$$

which is expected to be non-convex and affected by multiple local optima (Ogden et al., 2004).

GAs are well suited for the minimization of non-convex objective functions due to their ability to explore the entire search space looking for a global minima (Schmitt, 2004).

We adopt a steady-state GA, where a population of individuals is created sampling the search space. A temporary population is created at every generation and added to the previous one. The worst individuals are removed in order to maintain the size of the population constant. The roulette-wheel selection method was utilized with scaled fitness scores. Any individual has a probability $p$ of being chosen where $p$ is equal to the fitness of the individual divided by the sum of the fitnesses of all the individuals in the population. An initial population of 500–1000 individuals was used along with a mutation percentage of 0.01 and a crossover percentage of 0.6. Although the algorithm was set to terminate after 200–500 generations, it started to converge to a minima, which could be local or global, after approximately 80 generations.

## 4. Model validation

### 4.1. Monotonic tests on brain tissue

Uniaxial tests performed by Miller and Chinzei (2002) on short cylindrical samples of swine brain tissue are considered. These tests were performed in both tension and compression (Fig. 1), under different strain rates (*moderately high*, *intermediate* and *slow* strain rates). Brain samples were extracted between the arachnoid membrane and the ventricle surface of the swine brains, with a 30 mm diameter and a 13 mm height, in order to measure *averaged* isotropic properties of the tissue.

The experimental results by Miller and Chinzei (2002) can be summarized into five stress–strain curves (Miller et al., 2006), relating the first Piola–Kirchhoff traction $P_z$ (vertical force divided by the undeformed cross-sectional area) with the mean stretch $\lambda$ (current sample height $2h$ divided by the initial height $2H$, cf. Fig. 1). Two curves are in tension ($\dot{\lambda} = 0.64, 0.64\times10^{-2}\,\mathrm{s}^{-1}$), and three in compression ($\dot{\lambda} = 0.64, 0.64\times10^{-2}, 0.64\times10^{-5}\,\mathrm{s}^{-1}$).

A first set of parameter estimates was obtained through a viscoelastic fitting model (ve), ignoring the plastic part of the equilibrium network. We considered two relaxation mechanisms, one term Ogden models, and independent tensile and compressive responses. The selected fitting

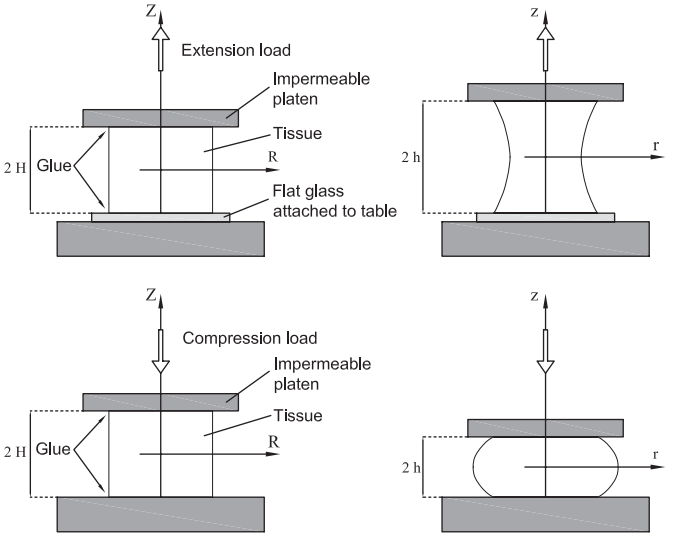


Fig. 1. Illustration of the uniaxial tests on short cylindrical samples of brain tissue by Miller and Chinzei (2002).

parameters are

$$\boldsymbol{p} = \{\mu_1, \alpha_1, \tau_1, \mu_{1,1}, \alpha_{1,1}, \tau_2, \mu_{2,1}, \alpha_{2,1}\} \quad (P = 8), \tag{4.1}$$

where

$$\tau_i = \frac{\eta_{i,1}^{\text{dev}}}{\mu_{i,1}} \quad (i = 1, 2) \tag{4.2}$$

denote the *relaxation times* of the viscous networks.

The tensile–compressive GA estimates are shown in the first two columns of Table 1. The positive $\{\mu, \alpha\}$ pairs in tension ($N^e = 2$), negative pairs in compression ($N^e = 3$), and significantly higher shear moduli $\mu^0$, $\mu^\infty$ in compression confirm the well known notion in the literature of the heterogeneous tensile–compressive nature of brain tissue (Miller and Chinzei, 2002; Prange and Margulies, 2002; Meaney, 2003; Velardi et al., 2006). A comparison between experimental and fitting stress–strain curves is shown in Fig. 2.

Table 1
GA material parameter estimates for (Miller and Chinzei, 2002) monotonic tests on brain tissue

| | Ten. ve | Comp. ve | Global ve | Global ve/ep |
|---|---|---|---|---|
| $t = \infty$ | | | | |
| $\mu_1$ (Pa) | 106.4 | −147.6 | −45.8 | −30.6 |
| $\alpha_1$ | 1.89 | −2.95 | −5.79 | −8.00 |
| $\mu^\infty$ (Pa) | 100.4 | 218.2 | 132.6 | 122.2 |
| $\tau_1$ (s) | 4.68 | 4.31 | 0.18 | 0.19 |
| $\mu_{1,1}$ (Pa) | 106.4 | −481.6 | −66.9 | −53.2 |
| $\alpha_{1,1}$ | 1.89 | −2.39 | −17.99 | −19.09 |
| $\tau_2$ (s) | 62.43 | 598.81 | 499.20 | 490.30 |
| $\mu_{2,1}$ (Pa) | 106.4 | −144.0 | −74.4 | −68.9 |
| $\alpha_{2,1}$ | 1.89 | −4.56 | −6.32 | −6.42 |
| $\mu^0$ (Pa) | 301.34 | 1122.7 | 969.9 | 851.8 |
| $\sigma_0$ (Pa) | – | – | – | 315.28 |
| $\varepsilon_0^p$ | – | – | – | 0.30 |
| $f$ (Pa) | 23.13 | 158.56 | 255.32 | 180.17 |

Further estimates were obtained for the mixed tensile–compressive response (*global response:* $N^e = 5$), alternatively considering a pure viscoelastic (ve), and a viscoelastic/elastoplastic (ve/ep) model. In the first case we proceeded as before, while in the second we activated the plastic section of the time-infinity network, assuming

$$\boldsymbol{p} = \{\mu_1, \alpha_1, \tau_1, \mu_{1,1}, \alpha_{1,1}, \tau_2, \mu_{2,1}, \alpha_{2,1}, \sigma_0, \varepsilon_0^p\} \quad (P = 10) \tag{4.3}$$

(plastic rate effects were deactivated).

The global GA estimates are shown in the third and fourth columns of Table 1, while the corresponding fitting curves are depicted in Fig. 3. It can be observed that the global response is best fitted with negative $\{\mu, \alpha\}$ pairs, and that the inclusion of plastic behavior significantly increases the fitness performance.

Miller and Chinzei (2002) estimated $\mu^0 = 156\,\text{Pa}$, $\mu^\infty = 842\,\text{Pa}$, $\alpha_1 = \alpha_{1,1} = \alpha_{2,1} = -4.7$, through a simplified "finite linear" viscoelastic modeling, accounting for large deformations and small perturbations away from thermodynamic equilibrium. Those results are in good agreement with the global GA estimates of Table 1. The same authors estimated $\tau_1 = 0.50\,\text{s}$ and $\tau_2 = 50.0\,\text{s}$, that is, a second relaxation time about 10 times smaller than our global estimates ($\tau_2 \approx 500\,\text{s}$, cf. Table 1). It is worth noting that our finite viscoelastic model converges more rapidly toward thermodynamic equilibrium than finite linear viscoelastic theories (Reese and Govindjee, 1998). This implies that larger relaxation times are needed in order to extend the viscous effects over time.

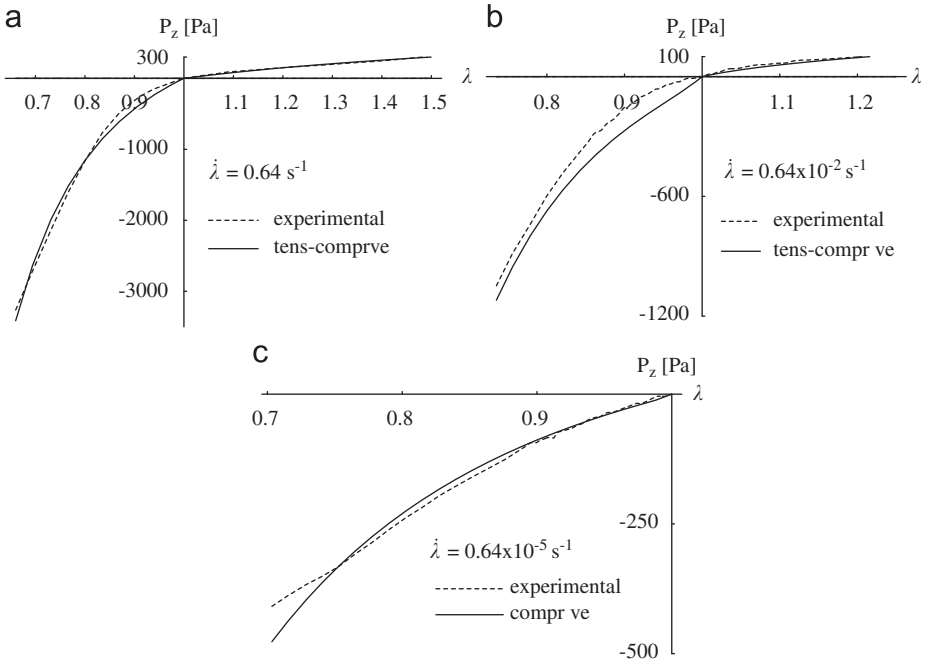


Fig. 2. Independent tension–compression viscoelastic fits of Miller and Chinzei (2002) experiments.

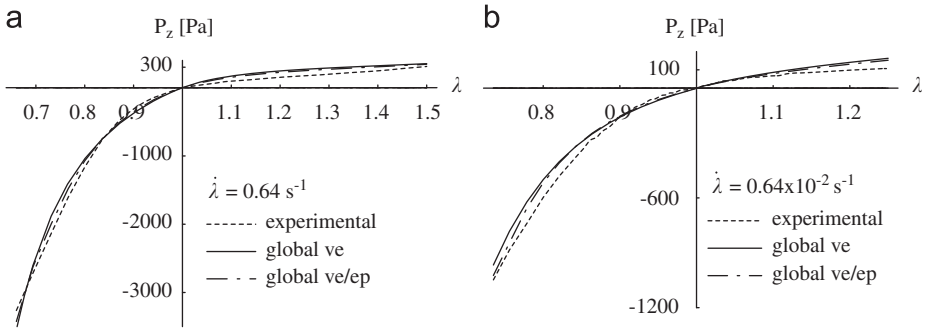


Fig. 3. Global viscoelastic (ve) and viscoelastic/elastoplastic (ve/ep) fits of Miller and Chinzei (2002) experiments.

Table 2
GA material parameter estimates for Franceschini et al. (2006) tests on specimens of brain white matter

| | Compression–tension | Tension–compression | Three cycles |
|---|---|---|---|
| $t = \infty$ | | | |
| $\mu_1$ (Pa) | −297.29 | −659.71 | −69.81 |
| $\alpha_1$ | −2.98 | −30.0 | −40.0 |
| $\mu^\infty$ (Pa) | 442.96 | 9895.96 | 1396.11 |
| $\tau_1$ (s) | 19.81 | 2.13 | 0.57 |
| $\mu_{1,1}$ (Pa) | −223.89 | −133.37 | −610.73 |
| $\alpha_{1,1}$ | −6.31 | −2.02 | −23.76 |
| $\tau_2$ (s) | 211.17 | 207.57 | 7.62 |
| $\mu_{2,1}$ (Pa) | 2.05 | 109.30 | −4.95 |
| $\alpha_{2,1}$ | 21.55 | 15.26 | −1.00 |
| $\tau_3$ (s) | – | – | 24.58 |
| $\mu_{3,1}$ (Pa) | – | – | 74.67 |
| $\alpha_{3,1}$ | – | – | 1.00 |
| $\mu^0$ (Pa) | 1171.41 | 10864.3 | 8691.45 |
| $\sigma_0$ (Pa) | 1273.64 | 81.32 | 91.64 |
| $\varepsilon_0^p$ | 1.0e−4 | 0.176 | 7.6e−4 |
| $n$ | 10.0 | 7.51 | 1.78 |
| $\dot{\varepsilon}_0^p$ | – | – | 0.01 |
| $m$ | – | – | 14.35 |

### 4.2. Cyclic uniaxial tests on brain tissue

A final set of estimates was obtained considering the cyclic quasistatic uniaxial tests performed by Franceschini et al. (2006) on human brain tissue excised during autopsy. We examined two one-cycle compression–tension (first compression and then tension) and tension–compression tests (Franceschini et al., 2006, Fig. 1), and a multi-cycle test (Franceschini et al., 2006, Fig. B.3) performed on prismatic specimens of white matter harvested from different brain regions. In the latter case, we analyzed the first three cycles of a 20 cycle test, activating three viscoelastic networks and plastic rate effects.

The GA material parameter estimates and a comparison between experimental and fitting curves are illustrated in Table 2 and Figs. 4 and 5. It is evident from the figures that our model is able to capture hysteresis, strong non-linearity, different behavior in tension and in compression, relaxation, preconditioning and cyclic softening of brain tissue. The results of Table 2 show that human brain samples analyzed by Franceschini et al. (2006) manifest higher initial and long term shear moduli in comparison with the pig brain samples tested by Miller and Chinzei (2002) (cf. Table 1).

## 5. Discussion and conclusions

We have demonstrated the ability of the presented material model to reproduce the behavior of swine and human brain tissue. The model combines finite viscoelasticity and finite elastoplasticity, decoupling of volumetric and deviatoric responses. The viscoelastic response is described through Ogden-type models including volumetric deformation. Deviatoric plasticity allows for reproducing shearing injures, like e.g. diffuse axonal damage in brain tissue. Volumetric plasticity is related to the expansion of voids or bubbles in the material (Ortiz and Molinari, 1992), as physically observed in soft biological tissues undergoing crazing, cavitation or both. Those specific features of the model are demonstrated by El Sayed et al. (2007).

The large number of material parameters required by the model demanded a systematic approach for their identification. We formulated an identification procedure based on genetic algorithms, and the flexibility and versatility of this method was demonstrated by calibrating parameters for brain tissue under different loading conditions.

The model presented herein is primed for use in the simulation of impact and wave induced damage in biological tissues. We address the application of this model to traumatic brain injury in a separate publication (El Sayed et al., 2007). Future work may include extending the model to anisotropy to account for directional mechanical response of tissues crossed by oriented or slightly dispersed fibers.

### Conflict of interest statement

There are no conflicts of interest of any kind in the work presented in the manuscript.

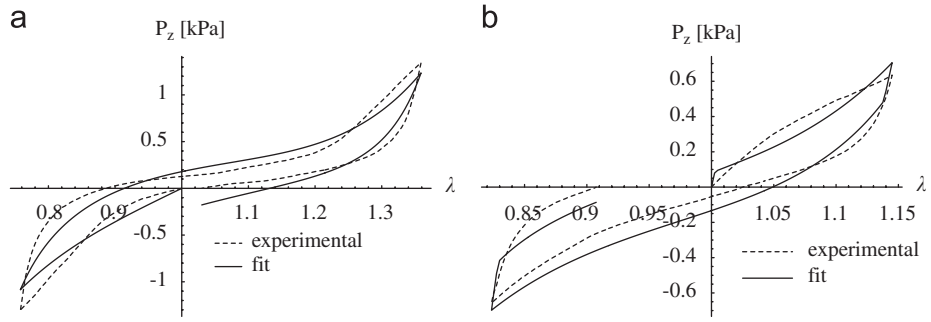


Fig. 4. The presented model fits of Franceschini et al. (2006) one-cycle compression–tension (a) and tension–compression (b) tests on specimens of white matter.

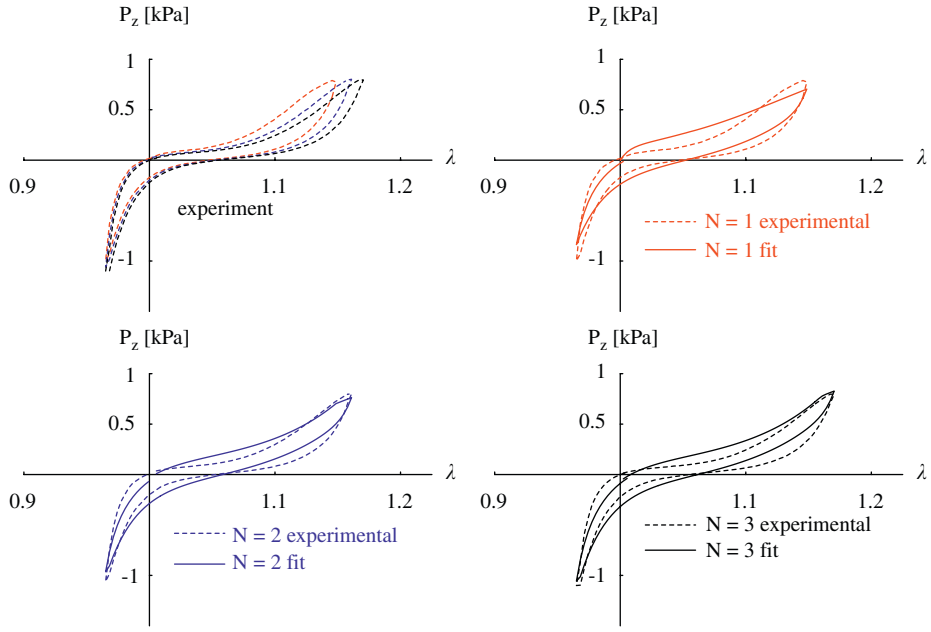


Fig. 5. Fits of Franceschini et al. (2006) cyclic tests on a specimen of white matter. (Fig. B.3, first three cycles.)

## Acknowledgments

The authors would like to thank Professor Francesschini and Professor Bigoni for their indispensable collaboration. Also, F.F. greatly acknowledges the support of the Italian Fulbright Commission and the Council for International Exchange of Scholars.

## Appendix A. Supplementary data

Supplementary data associated with this article can be found in the online version at 10.1016/j.jbiomech.2008.02.023.

## References

Adams, J.H., Graham, D.I., 1984. Diffuse brain damages in non-missile head injury. In: Recent Advances in Histopathology. Churchill Livingstone, Edinburgh.

Ball, J.M., 1977. Convexity conditions and existence theorems in nonlinear elasticity. Archive for Rational Mechanics and Analysis 63, 337–403.

Bergström, J.S., Boyce, M.C., 2001. Constitutive modeling of the time-dependent and cyclic loading of elastomers and application to soft biological tissues. Mechanics of Materials 33, 523–530.

Brands, D.W.A., Bovendeerd, P.H.M., Wisman, J.S.H.M., 2002. On the potential importance of non-linear viscoelastic material modelling for numerical prediction of brain tissue response: test and application. Stapp Car Crash Journal 46, 103–121.

Brennen, C.E., 2003. Cavitation in biological and bioengineering contexts. In: Fifth International Symposium on Cavitation, Osaka, Japan.

Ciarlet, P.G., 1998. Three-dimensional Elasticity. Elsevier, Amsterdam.

El Sayed, T., Mota, A., Fraternali, F., Ortiz, M., 2007. Biomechanics of traumatic brain injury (preprint). Division of Engineering and Applied Science, California Institute of Technology.

Fancello, E., Ponthot, J.P., Stainier, L., 2006. A variational formulation of constitutive models and updates in non-linear finite viscoelasticity. International Journal for Numerical Methods in Engineering 65, 1831–1864.

Franceschini, G., Bigoni, D., Regitnig, P., Holzapfel, G.A., 2006. Brain tissue deforms similarly to filled elastomers and follows consolidation theory. Journal of the Mechanics and Physics of Solids 54 (12), 2592–2620.

Gasser, T.C., Holzapfel, G.A., 2002. A rate-independent elastoplastic constitutive model for biological fiber-reinforced composites at finite strains: continuum basis, algorithmic formulation and finite element implementation. Computational Mechanics 29, 340–360.

Gasser, T.C., Ogden, R.W., Holzapfel, G.A., 2006. Hyperelastic modelling of arterial layers with distributed collagen fibre orientations. Journal of the Royal Society Interface 3, 15–35.

Govindjee, S., Reese, S., 1997. A presentation and comparison of two large deformation viscoelasticity models. Journal of Engineering Materials and Technology—Transactions of the ASME 119, 251–255.

Hardy, W.N., Khalil, T.B., King, A.I., 1994. Literature review of head injury biomechanics. International Journal of Impact Engineering 15, 561–586.

Holzapfel, G.A., 2001. Nonlinear Solid Mechanics: A Continuum Approach for Engineering. Wiley, England.

Holzapfel, G.A., Gasser, T.C., Ogden, R.W., 2000. A new constitutive framework for arterial wall mechanics and a comparative study of material models. Journal of Elasticity 61, 1–48.

Johnson, E.A.C., Young, P.G., 2006. The analysis of pressure response in head injury. In: C2006 Digital Human Modeling for Design and Engineering Conference, July 2006, Lyon, France. SAE Paper No. 2006-01-2368.

Lubock, P., Goldsmith, W., 1980. Experimental cavitation studies in a model headneck system. Journal of Biomechanics 13, 1041–1052.

Meaney, D.F., 2003. Relationship between structural modeling and hyperelastic material behavior: application to CNS white matter. Biomechanics and Modeling in Mechanobiology 1, 279–293.

Miller, K., 2005. Method of testing very soft biological tissues in compression. Journal of Biomechanics 38, 153–158.

Miller, K., Chinzei, K., 1997. Constitutive modeling of brain tissue: experiment and theory. Journal of Biomechanics 30, 1115–1121.

Miller, K., Chinzei, K., 2002. Mechanical properties of brain tissues in tension. Journal of Biomechanics 35, 483–490.

Miller, K., Taylor, W., Wittek, A., 2006. Mathematical models of brain deformation behaviour for computed-integrated neurosurgery. Research Report of Intelligent Systems for Medicine Laboratory, University of Western Australia, ISML/01/06.

Molinari, A., Mercier, S., 2001. Micromechanical modelling of porous materials under dynamic loading. Journal of the Mechanics and Physics of Solids 49 (7), 1497–1516.

Nusholtz, G.S., Glascoe, L.G., Wylie, E.B., 1996. Modeling cavitation during head impact. In: Proceedings of NATO/AGARD Head Impact Conference, Paper 6.

Ogden, R.W., 1984. Non-linear Elastic Deformations. Ellis Horwood, Chichester, UK.

Ogden, R.W., 2003. Nonlinear elasticity, anisotropy, material stability and residual stresses in soft tissue. In: Holzapfel, G.A., Ogden, R.W. (Eds.), Biomechanics of Soft Tissue in Cardiovascular Systems, CISM Courses and Lectures Series, vol. 441. Springer, Wien, pp. 65–108.

Ogden, R.W., Saccomandi, G., Sgura, I., 2004. Fitting hyperelastic model to experimental data. Computational Mechanics 34, 484–502.

Ortiz, M., Molinari, A., 1992. Effect of strain-hardening and rate sensitivity on the dynamic growth of a void in a plastic material. Journal of Applied Mechanics—Transactions of the ASME 59 (1), 48–53.

Perles, S.J., Rewcastle, N.B., 1967. Shear injuries of the brain. Canadian Medical Association Journal 96, 577–582.

Prange, M.T., Margulies, S.S., 2002. Regional, directional, and age dependent properties of the brain undergoing large deformation. Journal of Biomechanical Engineering—Transactions of the ASME 124, 244–252.

Reese, S., Govindjee, S., 1998. A theory of finite viscoelasticity and numerical aspects. International Journal of Solids and Structures 35, 3455–3482.

Schmitt, L.M., 2004. Theory of genetic algorithms II: models for genetic operators over the string-tensor representation of populations and convergence to global optima for arbitrary fitness function under scaling. Theoretical Computer Science 310, 181–231.

Stoyanovski, M., Grozeva, M., 2005. Current concepts on morphogenesis of craniocerebral injuries. Mini-review, Trakia University.

Strich, S.J., 1956. Diffuse degeneration of cerebral white matter in severe dementia following head injury. Journal of Neurology, Neurosurgery and Psychiatry 19, 163–185.

Velardi, F., Fraternali, F., Angelillo, M., 2006. Anisotropic constitutive equations and experimental tensile behaviour of brain tissue. Biomechanics and Modeling in Mechanobiology 5, 53–61.

Weinberg, K., Ortiz, M., 2005. Shock wave induced damage in kidney tissue. Computational Materials Science 32, 588–593.

Weinberg, K., Mota, A., Ortiz, M., 2006. A variational constitutive model porous metal plasticity. Computational Mechanics 37, 142–152.